UNCLASSIFIED

AD 405 814

DEFENSE DOCUMENTATION CENTER

FOR

SCIENTIFIC AND TECHNICAL INFORMATION

CAMERON STATION, ALEXANDRIA, VIRGINIA

UNCLASSIFIED

NOTICE: When government or other drawings, specifications or other data are used for any purpose other than in connection with a definitely related government procurement operation, the U. S. Government thereby incurs no responsibility, nor any obligation whatsoever; and the fact that the Government may have formulated, furnished, or in any way supplied the said drawings, specifications, or other data is not to be regarded by implication or otherwise as in any manner licensing the holder or any other person or corporation, or conveying any rights or permission to manufacture, use or sell any patented invention that may in any way be related thereto.

405 814

63-3-5

405814

TECHNICAL REPORT
HE-150-211

UNIVERSITY OF CALIFORNIA
INSTITUTE OF ENGINEERING RESEARCH
BERKELEY, CALIFORNIA

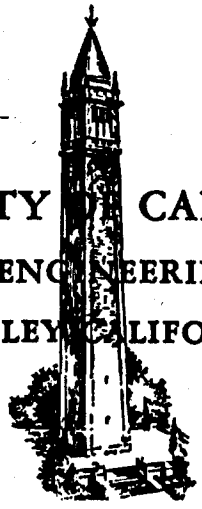

A SPECTROSCOPIC STUDY OF RECOMBINATION IN A HELIUM PLASMA

by

F. A. Robben

DDC
RECEIVED
JUN 10 1963
TISIA

SERIES NO. 132
ISSUE NO. 8
DATE April 5, 1963

CONTRACT AF 49(638)-502
SERIES NO. 132-7
REPORT NO. HE-150-211
APRIL 5, 1963

SPONSORED BY
AIR FORCE OFFICE OF SCIENTIFIC RESEARCH
AIR RESEARCH AND DEVELOPMENT COMMAND

A SPECTROSCOPIC STUDY OF RECOMBINATION IN A HELIUM PLASMA

by

F. A. Robben

A portion of a Ph.D. Thesis in Physics

Reproduction in whole or in part is permitted
for any purpose of the United States Government

FACULTY INVESTIGATORS:

F. S. SHERMAN, Associate Professor of Aeronautical Sciences

L. TALBOT, Associate Professor of Aeronautical Sciences

ABSTRACT

Recent work on ion-electron recombination has shown that a model involving recombination into highly excited bound levels through electron-electron-ion collisions and transitions between the bound levels through electron-atom collisions as well as the usual radiative processes, is in good agreement with experiment. By making absolute intensity measurements of all the lines of helium emitted from the decaying plasma of an arc jet in the visible and near ultraviolet, the number densities of the excited states of helium have been calculated. When interpreted by means of the collisional-radiative recombination model, these measurements give values for $K_{n,n-1}$, the collisional de-excitation rate constant of an excited helium atom from level n to $n-1$. The constancy of $K_{n,n-1}$ over a range of electron density from 4×10^{12} to 4×10^{14} per cm^3 indicates the validity of the model, and the values of $K_{n,n-1}$ are in reasonable agreement with a recent theory of classical excitation cross sections. A square root dependence of this cross section on the excess energy is indicated, since the values of $K_{n,n-1}$ appear to be independent of temperature. It is then found that $Q_{2,3} = 9.3 \times \sqrt{E}$, $Q_{3,4} = 73 \times \sqrt{E}$, and $Q_{4,5} = 380 \times \sqrt{E}$, where $Q_{n,n+1}$ is the averaged excitation cross section from the levels with principal quantum number n to the levels with principal quantum number $n + 1$ in units 10^{-15} cm^3, and E is the excess energy in ev. These cross sections have an estimated error of about 30% in the threshold energy range to about 0.3 ev.

TABLE OF CONTENTS

INTRODUCTION

Recent work on electron recombination with monatomic ions has rather successfully explained the increase in the recombination rate from the values given by radiative capture for low density plasmas to the much higher values generally observed in laboratory plasmas, with densities ranging from 10^{11} to 10^{14} ions/cm^3.[1,2,3,4] The two important processes not taken into account in the older work on the problem are electron capture and transitions between excited atomic levels, both with a free electron providing the energy balance. A full analysis requires knowledge of the cross sections for these collision phenomena for practically all of the excited levels of the atom, and lack of this information has been the principal stumbling block in developing this theory. However, it has been found that classical expressions for the ionization and excitation cross sections of an atom by an electron give recombination rates in quite reasonable agreement with experiment. The theory also predicts the number of atoms in each excited state, and one of the principal verifications[2] of the theory rests on the spectroscopic measurement of the density of these excited atoms in helium, and their agreement with the theory. In the present experiments on the decaying plasma of an arc jet this has been turned around, and the spectroscopic measurements of the density of the excited states of helium have been used to calculate the collisional transition rates. These are found to be in reasonable agreement with transitional rates calculated using recently derived classical cross sections,[5] in which the motion of the orbital electron is taken into account. Detailed calculations of the recombination rate using these cross sections have been given in reference 4, and some general

simplifications in the theory are discussed in references 2 and 3. First we will discuss the plasma source and the spectroscopic equipment, and then the technique used to obtain the density of an excited atomic level from the intensity of an atomic line. A general discussion of these experimentally determined densities is followed by a deduction of the collisional de-excitation rate constants for the excited levels, a comparison of these rate constants with those calculated using classical cross sections, and finally the calculation of the cross sections consistent with the experimental data.

EXPERIMENTAL EQUIPMENT

A schematic outline of the plasma jet wind tunnel[6] and the spectrograph is shown in Fig. 1. A 1/4 inch tungsten cathode was placed about two inches axially from a copper nozzle which served as the anode. The nozzle had a throat diameter of 0.44 inches, and all parts were water cooled. With a helium flow rate of 0.05 gm moles/sec and an arc current of 500 amperes, the pressure in the arc chamber was about 90 mm Hg and the arc voltage was about 33 volts. In most of the experiments a free jet expansion of the helium plasma was used, and the nozzle ended at the sonic throat. The main body of the wind tunnel, which contained a traverse mechanism for positioning various probes in the flow and a quartz window for the spectrograph, was maintained at about 0.25 mm Hg by a steam ejector pumping system.

The problem of a free jet expansion in an inviscid fluid has been analyzed,[7] and the solution indicates a rapid acceleration of the flow to a high Mach number, followed by a normal shock wave. The lower the pressure in the chamber in which the expansion occurs, the higher the Mach number reached before the shock wave. Unfortunately, because of its small atomic mass the helium flow has a low Reynolds number, so that the viscous corrections are large, and in fact under the conditions in these experiments inviscid flow theory cannot be applied to the expanding flow to determine the Mach number and other characteristics. This was borne out by a comparison of the axial variation of the spectroscopically measured electron densities with the gas densities deduced from measured impact pressures and isentropic flow theory. This measurement indicated that the Mach number never reached values much higher than 3.

It was not possible to run at higher flow rates to reduce these viscosity effects, as the arc voltage would break into oscillations of as much as 20 volts amplitude at a frequency of a few kilocycles, accompanied by similar oscillations in the luminosity of the plasma. At low flow rates all oscillations (up to about 100 megacycles) were either absent or small.

The temperature of the helium at the throat of the orifice can be estimated from the ratio of arc chamber pressure with and without arc operation. It can be shown that the mass flow through a sonic throat is proportional to $p_o/\sqrt{T_o}$, where p_o and T_o are the stagnation pressure and temperature, and a comparison of the measured stagnation pressures with and without arc operation gave a stagnation temperature of about 7000°K. The temperature, density, and pressure in the free jet expansion drop rapidly, although not as rapidly as predicted by isentropic flow theory, until the shock wave is reached, about four inches downstream. After the shock wave, which is quite diffuse, the plasma had a diameter of about six inches and appeared quite uniform to the end of the tunnel, four feet farther downstream. When the arc was operating "well", this plasma was remarkably stationary and symmetric, giving the appearance of a large glow discharge tube. At other times the jet was less symmetric, as the arc showed a tendency to attach itself to one side of the anode, and considerable flickering could be noticed in the boundaries of the jet.

The spectrograph used was a Jarrell Ash 3.4 meter Ebert type, which can take photographic spectra, or as was the case in these experiments, can be fitted with an exit slit and a photomultiplier and be operated as a direct recording instrument. Wavelength coverage was obtained by rotation of the grating, with readout on a counter directly in Angstroms. The radiation in a cross section of the plasma about 3.5 mm high and

0.5 mm wide (in the direction of flow) was thus incident on the slit of the spectrograph. The plane mirror swiveled on ball bearings about two axes with calibrated micrometer drives, so that any region of the plasma within about eight inches of the orifice could be observed. This plane mirror also rotated sufficiently so that various discharge tubes and radiation standards could be focused on the spectrograph.

A survey of the radiation from the helium plasma on photographic plates revealed only neutral helium atoms, with the Rydberg series merging into a continuum at about $n = 12$ for the region of the jet close to the orifice. Farther downstream the Rydberg series disappeared at about $n = 18$, and there was no observable continuum. With long exposure (10^4 times that necessary to observe the stronger lines of helium), N_2 and N_2^+ molecular bands were observed, principally in the boundary of the jet, and hydrogen and argon lines were observed more uniformly across the plasma. The nitrogen bands were probably due to air leaks in the tunnel, while the hydrogen and argon lines indicated that the gas purity was better than 100 parts per million. In particular, no tungsten or copper from the arc was found.

The argon impurity lines in helium show a peculiarity. When the arc is run on pure argon, only the lines belonging to argon I, the neutral atom, are found. This is presumably due, as in helium, to the fact that the more highly ionized species recombine very rapidly, before the plasma reaches the point of observation. However, the argon impurity lines in helium are all of argon II (singly ionized), with no argon I observable. It seems as if some process must very rapidly excite the ground state argon ions before they have a chance to recombine. One possibility is that collisions of the second kind with helium atoms in the $n = 2$ levels

may excite the ground state argon ions. Because of resonance radiation trapping, all of the n = 2 levels of helium will have fairly high densities, although considerably less than the electron density (because of collisional de-excitation). Since none of the observed argon ion lines had an excitation energy greater than 21.2 volts, the highest energy of the n = 2 helium levels, this process would seem to be indicated. In order to suppress the argon I radiation, it is necessary that the rate of excitation of the argon ions be considerably greater than their rate of recombination. Upon estimating the recombination rate (from the theory presented in this paper) and assuming the resonance radiation trapping to be complete so that the density of helium atoms in the n = 2 levels can be calculated assuming collisional de-excitation, it is found that the cross section for excitation of an argon ion in a collision with an excited helium atom must be considerably greater than 10^{-14} cm^2. In view of such a large cross section, this explanation must be regarded as only tentative.

The measurement of the radiation intensity from a region of plasma in the jet cannot be made directly, since observations on the centerline of the plasma jet, for instance, include contributions from all regions out to the boundary. If the jet is assumed to be cylindrically symmetric, the radiation reaching the spectrograph is given by the Abel integral equation, whose inversion is well known. This inversion requires the complete profile of the intensity of each line across the jet, thus the intensity of each helium line was recorded as the movable plane mirror, driven by a motor, performed a transverse scan of the jet. A Moseley x-y recorder, with x-axis coupled to the mirror, was used to record this scan. The exit slit of the spectrometer was set at 0.71 mm and the entrance slit at 0.13 mm, so that quite uniform response was achieved over a

wavelength range of 3.4 A, for reasons discussed later. This spectral response was determined by scanning a singlet helium line from a discharge tube. (It might be noted that adjustment of the RCA 1P28 photomultiplier tube behind the exit slit was required to find a region of the photocathode with uniform response.)

The intensity calibration of the spectrograph-photomultiplier system was made with a tungsten ribbon filament lamp, viewed with the same optical arrangement as the plasma except for the quartz window in the tunnel. The primary standard, made by General Electric (#30A/T 24-3), and equipped with a quartz window, was supplied by the Bureau of Standards and calibrated for spectral intensity from 2500 A to 7500 A, when run at 35.0 amperes AC. This lamp was used only occasionally, and another identical lamp calibrated against the primary standard was used for normal operation. The measurement of current had to be quite precise, as an error of 0.3% in current gave a noticeable change in intensity. The ammeter was periodically checked against a laboratory standard accurate to 0.1%. Scattered light from the internal parts of the spectrograph necessitated the use of a U.V. transmitting, visible absorbing filter for calibration below 3400 A. With this filter, Corning 7-54, the calibration was extended to 2500 A, with about 65% scattered light at 2500 A. A red transmitting filter, Corning 2-73, was used to eliminate the second order radiation for wavelengths larger than 6000 A. The whole system had less than 2% variation in sensitivity over periods of several days. The photomultiplier was powered by batteries and left on continuously, and only currents less than 10^{-6} amperes were drawn from it to minimize fatigue effects.

A complete set of measurements of all observable lines of helium required about 1-1/2 hours, and during this time the plasma jet was generally quite steady. The intensity of any given line of helium varied by less than 5% if the arc current was maintained constant, while the arc voltage would typically drop about 10%. The largest errors in the final results probably arise from the fact that small errors in measurement, or in lack of symmetry of the jet, have a large effect on the Abel integral inversion.

If there is no self absorption the equation describing the radiation $J(x)$ observed by the spectrograph in a predetermined wavelength interval is given by

$$J(x) = \int_x^R \frac{I(r)\ 2r\ dr}{(r^2-x^2)^{1/2}} \tag{1}$$

where $I(r)$ is the intensity of emission of the jet, in watts/cm^3, assumed to be a function of radius only, and $J(x)$ is the energy detected by the spectrograph in watts/cm^2, when aimed at distance x from the jet center. (See Fig. A1) The inversion of this Abel equation is given by

$$I(r) = \frac{1}{\pi} \int_r^R \frac{\frac{dJ(x)}{dx}\ dx}{(x^2 - r^2)^{1/2}} \tag{2}$$

Numerical solutions based on Eq. (2)[8,9,10] have been described in the literature. The experimental points which represent the curve of $J(x)$ obtained in the transverse scan of the jet are fitted with an interpolating function, either directly or by some least-square curve fitting technique, so as to preserve maximum accuracy. Three different interpolating methods for the experimental points were tried, a linear fit to

two points at a time,[8] a cubic fit to four points at a time,[9] and a six term Fourier cosine series fitted to twenty points.[11] By use of a function which approximated our experimental curves in shape, and whose analytic inversion was obtained, the accuracies of these various methods were tested, while varying the total number of points representing $J(x)$ from 5 to 20, and the accuracy of each point from four significant figures to two significant figures. In Appendix A a detailed discussion of these procedures is given. For two significant figures, which represent the relative accuracy of our experimental measurements, it was found that the cubic fit to about five points was as accurate as any method tried, and therefore was used for the data reduction in these experiments. A relative error of 1% in the first two or three points near the centerline of $J(x)$ would result in about a 5% error in $I(r)$ on the centerline. Since the experimental curves were, at best, of this order of symmetry, a 5% error is about the best obtainable on the centerline. The two halves of the experimental curves $J(x)$ were averaged together before the data reduction in most of the experiments. The numerical work was done on an IBM 7090 computer, with Eq. (2) put in the form

$$I_m = \frac{1}{Nh} \sum_{n=0}^{N} J_n Z_{n,m} \tag{3}$$

where $r = mh$, $x = nh$, and $Z_{n,m}$ was, for the cubic and linear fits, a triangular matrix. For the six term Fourier series expansion $Z_{n,m}$ is a 20 term square matrix.

The intensity of an atomic line, in ergs/(cm^3-sec-steradian), is given by

$$I_{u\ell} = N_u \frac{A_{u\ell}}{4\pi} h\nu \qquad (4)$$

where N_u is the number/cm^3 of atoms in the upper state, $A_{u\ell}$ is the Einstein emission coefficient from state u to state ℓ in sec^{-1} (averaged over all sub-levels), and $h\nu$ is the energy of the quantum of radiation in ergs. If the signal from the photomultiplier of the spectrometer, when set at wavelength λ to measure radiation from states $u - \ell$, is called $R_{u\ell}(\lambda)$, then the values of J_n to be used in Eq. (3) will be given by

$$J_n^{u\ell} = \frac{R_{u\ell}(\lambda)\, W}{S(\lambda)} \quad , \qquad (5)$$

where $R_{u\ell}(\lambda)$ is measured at points whose distance from the center of the plasma is nh. As shown in Appendix B, W is the spectral band pass (the spectrometer has approximately uniform response over a range of wavelength W, and zero response outside of this region), and $S(\lambda)$, the spectral sensitivity is given by

$$S(\lambda) = \frac{R^\circ(\lambda)}{I^\circ(\lambda)} \qquad (6)$$

Here $I^\circ(\lambda)$ is the spectral steradiancy of the standard lamp and $R^\circ(\lambda)$ is the signal measured when the spectrometer is focussed on the standard lamp.

To find the desired quantity, N_u, in Eq. (4), theoretical values of the Einstein coefficient, $A_{u\ell}$, must be used. Generally, theoretical workers give the oscillator strengths, $f_{\ell u}$, which are related to the

Einstein coefficients by the expression

$$g_u A_{u\ell} = \frac{8\pi^2 e^2}{mc\,\lambda^2} g_\ell f_{\ell u} \quad , \tag{7}$$

where g_u and g_ℓ are the multiplicities of the upper and lower states, and e, m, c, and λ are in cgs units. The values found by the coulomb expansion method of Bates and Damgaard[12] and the variational technique of Trefftz, et.al.[13] agreed quite closely, and were used as the basis of our values. The tables of Bates and Damgaard give values for all six series of lines in the visible up to $n = 5$ or 6, and Trefftz, et.al. calculated a number of the astrophysically important oscillator strengths, with some values at $n = 10$. These values were extrapolated graphically to give all oscillator strengths up to $n = 15$ by using the hydrogen oscillator strengths for the same series as a guide, and the resulting values used in this work are given in Table I.

The final expression for N_u/g_u is given by combining Eqs. (3), (4), (5), and (7), and results in

$$N_u/g_u = \frac{6.35 \times 10^6 \times W \times \sum_{n=0}^{N} J_n' Z_{nm}}{S(\lambda) \times E(\lambda) \times f_{\ell u} \times h} \tag{8}$$

where W is the spectral band pass in Angstroms, J_n' is the photomultiplier current in units of 10^{-8} amp for the transition $u \rightarrow \ell$, and $S(\lambda)$ is the spectral sensitivity of the spectrometer in units of 10^{-8}amp/(microwatts/[steradian-millimicron-mm^2]). E is given by $0.662 \times g_\ell/\lambda^3$, with λ in microns, $f_{\ell u}$ is the oscillator strength, and h is the interval in cm between the values of J_n.

RESULTS

Measurements were made on all the lines of helium that could be observed, and some of the transitions responsible for these lines are indicated on the energy level diagram shown in Fig. 2. The centerline values of N_u/g_u from Eq. (8) were plotted on a logarithmic scale versus the energy level, as shown in Figs. 3 and 4. These graphs are similar to those obtained by Hinnov and Hirschberg,[2] and, as was the case with their results, all the states of higher excitation seem to fall on a straight line, indicating a Boltzmann distribution whose temperature is given by the slope. The Boltzmann distribution arises from the fact that transitions between the levels induced by electron collisions are much more rapid than the net rate of recombination, a result leading to an estimate of the cross section in agreement with the results to be presented later.

For the lower levels, even though they deviate from a Boltzmann distribution, it appears that all levels with the same principal quantum number are approximately maintained with relative populations given by a temperature equal to that found from the higher levels. The 3^3S and 4^3S levels seem to deviate the most from this relationship, but an error in the oscillator strengths for these levels could change the results. It seems, then, that collisionally induced transitions between the triplet and singlet states belonging to the same quantum numbers must be fairly frequent, compared to the rate at which transitions occur from other levels. The general overall agreement of results from the different series for the higher levels indicates that the oscillator strengths used in the data reduction are accurate to at least about 10%, and that the measurements themselves are accurate to about 10%.

The high quantum number levels are also assumed to have rapid transitions induced by electron collisions with levels lying above the ionization limit, that is, with the free electrons. Thus, the whole system of upper levels is in equilibrium with the free electrons, and the Saha equation,

$$\frac{N_e N_i}{N_u} = \frac{g_i g_e}{g_u} \left(\frac{2\pi m_e kT}{h^3} \right)^{3/2} e^{-E_u/kT} , \qquad (9)$$

can be used to give the density of the free electrons. Upon setting $N_e = N_i$ and inserting numbers, Eq. (9) becomes

$$N_e = (1.2 \times 10^{22} T^{3/2} N_\infty/g_\infty)^{1/2} ,$$

where N_e is in electrons/cm^3, T is in ev, and

$$N_\infty/g_\infty = N_u/g_u \, e^{-E_u/kT} .$$

The quantity N_∞/g_∞ is found graphically by the extrapolation of the upper levels in Figs. 3 and 4 with a straight line to the $E = 0$ axis. The electron densities and temperatures obtained are given on the figures.

The Abel integral inversion, Eq. (2), can be considered as finding the mean depth of plasma, which is divided into the intensity measured by the spectrometer to give the intensity per unit volume of the plasma. For the higher principal quantum numbers this mean plasma depth should be a smooth function of quantum number only, since all levels belonging to a given quantum number are in equilibrium with each other. A plot was made of this mean depth versus principal quantum number, and a smoothing curve passed through the points. The results of the Abel integral inversion

were then adjusted so that the mean depth for each spectral line was that given by the smoothing curve. In some instances this procedure yielded appreciably less scatter in the plots of N_u/g_u vs. energy. Figure 3 was treated in this manner, while Fig. 4 was not. In most cases the points were not adjusted more than 10%, and also the mean depth of the plasma did not generally vary by more than 30% over all the lines.

The lines with high quantum number lying near the continuum approach 3 A in width, and the assumption that the line width is less than the spectral slit width, made in deriving Eq. (5), is no longer true. For these lines a spectral scan was made, with the spectrometer focused on the axis of the plasma column, and the area under the resulting curves was measured with a planimeter to find the intensity. The mean plasma depth as described previously was then used to find the number of atoms in the upper levels. These values are the points in Figs. 3 and 4 for n greater than 10, and while they seem to be a little below the equilibrium value, this is probably due to experimental error.

Two independent verifications of the electron density were attempted. First, the Stark broadening of the H_δ line ($n = 4$), when about 1% hydrogen was added to the helium, was measured. The half-width of the 3'P helium line was also measured and compared with a discharge tube to estimate the temperature of the atoms in the plasma, and the half-width of H_δ minus the instrumental and Doppler half-widths was called the half-width due to Stark broadening. The electron density was then calculated using the results on hydrogen line broadening of Griem, Kolb, and Shen,[14] and Table II gives some results. The rather poor agreement is not unreasonable in view of the large errors in the half-width measurements, lack of correction for spatial nonuniformity, and the simple

subtraction of the various half-widths. Particularly in the lower density case, the instrumental half-width makes a large correction. Secondly, the Inglis-Teller relation[15]

$$N_e = \frac{0.027}{2a_o^3 n^{7.5}}$$

where a_o is the Bohr radius, 0.53×10^{-8} cm, and n is the quantum number of the highest observable discrete level before the lines merge into a continuum, was used. This formula was derived on the basis of the Stark broadening of the highly excited states of hydrogen, but should be expected to apply to helium. Table II shows the results of this calculation, and it can be seen that the densities are in good agreement with the values from the Saha equation. Consideration of random errors leads to a probable error of about 15% in the values of electron density from the Saha equation.

The analysis of the recombination process follows the same model as employed in references 2, 3, and 4. A rate equation is written down for each level of principal quantum number n, taking into account both radiative processes and collisional processes involving electrons.

These equations are given by

$$\frac{dN_n}{dt} = \sum_{m=n+1}^{\infty} N_m A_{m,n} - N_n \sum_{m=1}^{n-1} A_{n,m}$$

$$+ N_e \left\{ \sum_{m=n+1}^{\infty} (N_m K_{m,n} - N_n K_{n,m}) - \sum_{m=1}^{n-1} (N_n K_{n,m} - N_m K_{m,n}) \right\} , \qquad (10)$$

where $K_{m,n}$ is the collisional rate constant for the transition from level m to n. The absorption of radiation is not explicitly included, but will later be taken into account by dropping all radiative transitions to the ground level, and the sums over the discrete levels can be generalized to include the continuum. For the plasmas considered here, N_e is much larger than any N_n except N_1, the ground level, and the parameters of the plasma such as temperature and density change slowly enough in time so that all the dN_n/dt except dN_1/dt in the complete set of Eqs. (10) can be set equal to zero. By then making some reasonable approximations regarding the nature of $K_{m,n}$ and using the experimental measurements as summarized in Figs. 3 and 4, values of $K_{m,m-1}$ can be obtained for those levels which are important in determining the recombination rate. This method depends on knowledge of the Einstein coefficients, and knowledge of the approximate behavior of $K_{m,n}$.

Recently Gryzinski[5] has calculated cross sections for excitation of atomic levels by electron impact from classical considerations that appear to be in fair accord with experiment. The excitation rate can be written in terms of the cross section as

$$N_e K_{n,m} = \int_{E_{ex}}^{\infty} \frac{dN_e(E)}{dE} v(E) Q_{n,m}(E) dE$$

where E_{ex} is the excitation energy of the level, $dN_e(E)/dE$ is the electron energy distribution, $v(E)$ is the electron velocity, and $Q_{n,m}(E)$ is the excitation cross section. The principle of detailed balance, which states that at equilibrium the forward and reverse rates of all possible reactions are equal, implies that

$$N_e N_n K_{n,m} = N_e N_m K_{m,n}$$

when all the constituents of the reaction are at thermodynamic equilibrium. Using the equilibrium values of N_n and N_m at temperature T and the Boltzmann distribution for $dN_e(E)/dE$ and $v(E)$, the de-excitation rate coefficient, in terms of the excitation cross section, can be shown to be

$$G_{m,n} \equiv g_m K_{m,n} = \frac{g_n}{\sqrt{\pi m_e}} \left(\frac{2}{kT}\right)^{3/2} \int_0^\infty (E+E_{ex})\, e^{-E/kT}\, Q_{n,m}(E+E_{ex})\, dE \quad , \qquad (11)$$

In terms of this expression Eq. (10), with $dN_n/dt = 0$, can be rewritten as

$$\sum_{m=n+1}^{\infty} G_{mn}\, D_{m,n} = L_n + \sum_{m=1}^{n-1} G_{n,m}\, D_{n,m} \quad , \qquad (12)$$

where

$$D_{m,n} = N_m/g_m - N_n/g_n \exp\,[(E_n-E_m)/kT]$$

and

$$L_n = (1/N_e)\,[N_n \sum_{m=1}^{n-1} A_{nm} - \sum_{m=n+1}^{\infty} N_m\, A_{mn}] \quad .$$

Calculations of $G_{m,n}$ using Gryzinski's cross sections show that the following approximations,

$$G_{m,m-2} \simeq 0.24 \quad G_{m,m-1}$$

$$G_{m,m-3} \simeq 0.10 \quad G_{m,m-1}$$

$$G_{m+1,m-1} \simeq 0.03 \quad G_{m,m-1}$$

are obeyed for all n of interest. Using these approximations and neglecting $G_{m+1,m-1}$ and all other collisional transitions, Eq. (12) can be written as

$$G_{n+1,n}\,(D_{n+1,n} + \Delta_{n+1,n}) = L_n + G_{n,n-1}\,D_{n,n-1} \qquad (13)$$

where

$$\Delta_{n+1,n} = 0.24 \times D_{n+2,n} + 0.10 \times D_{n+3,n} \quad .$$

The factors $D_{n+1,n}$, $\Delta_{n+1,n}$, and L_n can be determined from the experimentally measured densities of the various levels for $n \geq 3$. The method of obtaining $G_{n+1,n}$ then consists of estimating $G_{3,2}$ (in some cases this term is negligible), and solving Eq. (13) for $G_{4,3}$. This value of $G_{4,3}$ is then used to solve the equation for $n = 4$, etc., until the terms $D_{n+1,n}$ become zero as the density of level n approaches equilibrium with the free electrons.

In the calculation of the radiative factor L_n in Eq. (13) the terms involving radiation to the ground level are dropped, as the radiation is trapped. Assuming Doppler broadened lines (Stark and collision broadening are negligible), the spectral absorption coefficient at the line center in $cm^{-1}\ atm^{-1}$ is given by[16]

$$p(0) = S_{\ell u}\left(\frac{mc^2}{2\pi kT}\right)^{1/2}\frac{1}{\omega} \qquad (14)$$

where $S_{\ell u}$ is the integrated absorption coefficient in $cm^{-2}\ atm^{-1}$ and related to the absorption oscillator strength by[16]

$$S_{\ell u} = 2.38 \times 10^7\ f_{\ell u} \quad .$$

In Eq. (14) m is the atomic mass, and ω is the reciprocal wavelength of the transition in cm^{-1}. For the helium resonance transition $1^1S - 2^1P$ at 537 A, $f_{\ell u} \simeq 0.072$. Assuming typical conditions in the plasma jet, $T = 1000°K$ and 1.7×10^{17} atoms in the ground state, the absorption at line center given by Eq. (14) is found to be $50\ cm^{-1}$. Thus the mean free path of resonance radiation at the line peak is about 0.2 mm, so that to a good approximation in Eq. (13) the resonance radiation can be neglected compared to the other terms.

The results of this calculation of $G_{n,n-1}$ are shown in Fig. 5, as well as the values calculated using Gryzinski's cross sections with averaged energies of the helium levels. The value of $G_{3,2}$, important at the higher electron densities, was adjusted so as to bring all the points into reasonable agreement. Agreement with the classical theory is quite good; however, it appears to give values somewhat too large for the levels with $n > 5$, and somewhat too small for levels with $n < 4$. The relative constancy of $G_{n,n-1}$ over a factor of 100 in electron density can be regarded as a verification of the model of recombination.

The rate of recombination, according to the model, is given by

$$-\frac{dN_e}{dt} = \sum_{m=3}^{\infty} N_m A_{m,2} + N_e G_{3,2} (D_{3,2} + \Delta_{3,2}) \quad , \qquad (15)$$

with the radiative term being dominant in all cases except those with the highest electron density. As stated previously, resonance radiation to the ground level is neglected as it is trapped. In Table III the recombination coefficient α as defined by

$$-\frac{dN_e}{dt} = \alpha N_e^2$$

is given for most of the experiments, using the results of Eq. (15). Values of α interpolated from the table of Bates, Kingston, and McWhirter[4] for trapped resonance radiation, and from the graph given by Hinnov and Hirschberg,[2] are shown in Table III for comparison. These values depend on the experimentally determined T_e and N_e. The values of Bates, et.al., are about a factor 2 greater than the experimental values from Eq. (15), a somewhat surprising result. Their calculations were based on the same model of recombination used in the data reduction and used Gryzinski's expression for the collision cross sections, so it would seem that the two results should agree, within random errors of 50% or so. The use of Einstein coefficients for hydrogen instead of helium, and the differences in the collision cross section found by the present experiment, should make only a small correction.

The results of Hinnov and Hirschberg are a more approximate calculation, still based on the same model of recombination, using collisional cross sections estimated from the classical ionization cross section and the oscillator strengths of the allowed optical transitions. They were made for helium, and agree with their experimental measurements on the recombining helium plasma in a stellarator with an error of less than 50%. Their values are also generally somewhat greater than those of the present experiment.

The temperature dependence of the de-excitation rate constant, Eq. (11), is related to the form of the excitation cross section, $Q_{n,m}(E+E_{ex})$. If we assume that

$$(E+E_{ex})\, Q_{n,m}\,(E+E_{ex}) \sim E^{k}$$

then it is easy to show that

$$G_{m,n} \sim T^{k-1/2}$$

An examination of the experimental data plotted in Fig. 5 reveals no systematic variation of $G_{m,n}$ with electron temperature, indicating that $k = 1/2$ for the range of electron energy around kT. With the approximation that $kT \ll E_{ex}$, the expressions given in Table IV can be calculated for the average excitation cross sections. This excitation cross section must be considered to be a sum over all the levels belonging to the upper principal quantum number, and an average, according to the distribution, over all the levels belonging to the lower quantum number. Theoretical considerations[17] show that these cross sections have a square root dependence on E near $E = 0$, and the results given here are consistent with this behavior up to an energy of about 0.3 ev. Assuming, then, this dependence on E from threshold up to an energy of about 0.3 ev, the values of the proportionality constants in Table IV have an estimated error of about 30%.

The classical cross section derived by Gryzinski[5] applies to the energy transfer between two free electrons. The expression given by his Eq. (23), when written in the form $\sigma(E_1,\Delta E,E_2)\, d(\Delta E)$, is the cross section for excitation of an electron with energy E_1 to an energy between $E_1 + \Delta E$ and $E_1 + \Delta E + d(\Delta E)$, in a collision with another electron of energy E_2. The direction of the velocity of electron 1 has been assumed to be isotropic in space, and collisions with long interaction times have been neglected. In applying the above results to excitation of an atom, the bound electron is assumed to be in a circular

Bohr orbit, from which the kinetic energy E_1 can be found. The cross section for excitation of a level with principal quantum number n to level m is thus given by

$$Q_{n,m} = \sigma(E_1,\Delta E,E_2)(E_{m+1}-E_m)$$

where ΔE is the excitation energy, E_m-E_n, of the level, and E_{m+1} is the energy of the level in the same series with principal quantum number m + 1. This form gives the threshold variation of the cross section as $(E_2-\Delta E)^{1/2}$, in agreement with the quantum mechanical considerations. Use of this cross section to calculate $G_{n,n-1}$ results in fair agreement with the experiment, as already shown in Fig. 5. It appears, though, that the calculated value of $Q_{2,3}$ is too small by a factor of 3, and for the higher quantum numbers the calculated value may be somewhat too large. It might be expected from correspondence principle arguments, that the classical cross section would be asymptotic to the actual values at large quantum number. In this case, however the whole problem should be re-considered. It is possible to put the model of recombination in a classical framework, and then changing these equations to a quantum mechanical form by use of the correspondence principle may not lead to exactly the same cross section as indicated above.

The cross section for excitation of hydrogen from the ground 1S level to the 2P level has recently been measured by atomic beam methods[18] in the energy range near threshold, and the results fit the curve

$$Q_{1,2}(E+E_{ex}) = 0.29\ E^{1/2} \qquad (16)$$

for energies up to 3 ev. Results for excitation from 1S to 2S have also been determined,[19,20] and although they have not been shown to fit a curve of the form of Eq. (16), the cross section appears to be somewhat less than that of Eq. (16). It is interesting to note that this value for hydrogen agrees quite well with Gryzinski's theory. If it is true that the excitation cross sections for hydrogen and helium are about the same for the higher quantum numbers, then it appears that Gryzinski's theory gives about the correct results for Q_{1-2}, a factor 3 too low for Q_{2-3}, and again about the correct result for Q_{3-4} and Q_{4-5}.

SUMMARY

Detailed measurements of the number density of the excited levels of helium in a recombining plasma have been shown to be in good agreement with the collisional-radiative model of recombination. These measurements led to a determination of the average excitation cross section of several levels of helium in the threshold range to 0.3 ev excess energy which are proportional to the square root of the excess energy, as suggested by quantum mechanical calculations. These cross sections are also in approximate agreement with values calculated by the classical expression of Gryzinski.[5] The tables of recombination coefficient calculated by Bates, Kingston, and McWhirter[4] are in approximate agreement with the recombination coefficient inferred from experiment, as expected, since Bates, et.al., used Gryzinski's cross section in their calculations.

REFERENCES

1. R. G. Giovanelli, Australian J. Sci. Research A1, 274, 289 (1948); N. D'Angelo, Phys. Rev. 121, 505 (1961).
2. E. Hinnov and J. G. Hirschberg, Phys. Rev. 125, 795 (1962).
3. Byron, Stabler, and Bortz, Phys. Rev. Letters 8, 376 (1962).
4. Bates, Kingston, and McWhirter, Proc. Roy. Soc. 267A, 297 (1962) and 270A, 155 (1962).
5. M. Gryzinski, Phys. Rev. 115, 374 (1959).
6. Brundin, Talbot, and Sherman, "Flow Studies in an Arc Heated Low Density Supersonic Wind Tunnel," Univ. of Calif. Eng. Proj. Report HE-150-181 (1960).
7. K. Bier and B. Schmidt, ZAMP 13, 493 (1961); P. L. Owen and C. K. Thornhill, "The Flow in an Axially-Symmetric Supersonic Jet From a Nearly-Sonic Orifice into a Vacuum," ARC R and M 2616, Great Britain (1952).
8. O. H. Nestor and H. N. Olsen, SIAM Review 2, 200 (1960).
9. K. Bockasten, J. Opt. Soc. Am. 51, 943 (1961).
10. M. P. Freeman and S. Katz, J. Opt. Soc. Am. 50, 826 (1960).
11. Private Communication from J. B. Schumaker, Jr., of the National Bureau of Standards.
12. D. R. Bates and A. Damgaard, Phil. Trans. Roy. Soc. London 242A, 101 (1949).
13. Trefftz, Schlüter, Dettmar, and Jorgens, Z. Astrophys. 44, 1 (1957).
14. Griem, Kolb, and Shen, U. S. Naval Research Lab. Report 5805 (1962).
15. D. R. Inglis and E. Teller, Astrophys. J. 90, 439 (1939).
16. S. S. Penner, Quantitative Molecular Spectroscopy and Gas Emissivities (Addison-Wesley, Reading, Mass., 1959) p. 31.

17. M. J. Seaton, Atomic and Molecular Processes, ed. by D. R. Bates, (Academic Press, New York, 1962) p. 374.

18. Fite, Stebbings, and Brackman, Phys. Rev. 116, 356 (1959).

19. W. Lichten and S. Schultz, Phys. Rev. 116, 1132 (1959).

20. Stebbings, Fite, Hummer, and Brackman, Phys. Rev. 119, 1939 (1960).

21. P. M. Morse and H. Feshbach, Methods of Theoretical Physics (McGraw Hill, New York, 1953) Vol. I, p. 905.

22. V. Volterra, Theory of Functionals and of Integral and Integro-Differential Equations (Dover, New York, 1959) p. 55.

23. E. U. Condon and G. H. Shortley, The Theory of Atomic Spectra (Cambridge Univ. Press, Cambridge, 1959) p. 79.

TABLE I

HELIUM OSCILLATOR STRENGTHS

All values of $f_{\ell u}$ in units of 10^{-2}

Principal Quantum Number	2^3P-n^3D	2^1P-n^1D	2^3P-n^3S	2^1P-n^1S	2^3S-n^3P	2^1S-n^1P
3	62.3	72.5	5.71	16.5	7.64	4.64
4	12.3	12.1	2.08	5.08	1.16	0.824
5	4.67	4.31	1.19	2.29	0.385	0.300
6	2.33	2.05	0.709	1.26	0.190	0.151
7	1.32	1.15	0.414	0.720	0.114	0.087
8	0.849	0.740	0.268	0.465	0.071	0.055
9	0.580	0.490	0.186	0.311	0.048	0.037
10	0.408	0.351	0.131	0.223	0.034	0.026
11	0.300	0.280	0.099	0.168	0.025	
12	0.225	0.195	0.077	0.129	0.018	
13	0.175	0.152	0.060	0.103	0.014	
14	0.140	0.120	0.049	0.083		
15	0.112	0.098	0.039	0.069		

TABLE II

COMPARISON OF ELECTRON DENSITY

N_e from Saha Eq. cm^{-3}	T_e ev	Total 1/2 width of H_δ A	T_{plasma} from width of 3^1P ev	Stark 1/2 width of H_δ A	N_e from Stark Broadening cm^{-3}	n, last observable line	N_e from Inglis-Teller relation cm^{-3}
4.4×10^{14}	0.30	1.04	0.24	0.88	1.2×10^{14}	13	4×10^{14}
6.6×10^{13}	0.17	0.18	0.11	0.07	2.5×10^{12}	16	8×10^{13}

TABLE III

COMPARISON OF RECOMBINATION RATE

N_e cm^{-3}	T_e ev	α in 10^{-11} cm^3 sec^{-1}		
		from present experiment	from Bates, et. al.	from Hinnov and Hirschberg
4.2×10^{12}	0.15	5.8	14	13
1.6×10^{13}	0.28	1.9	3.3	1.5
1.9×10^{13}	0.15	30	68	58
2.6×10^{13}	0.13	89	150	130
6.6×10^{13}	0.17	34	65	111
4.4×10^{14}	0.29	25	33	13

TABLE IV

EXCITATION CROSS SECTION FOR HELIUM ATOMS

Averaged over all levels with principal quantum number n and summed over all levels with principal quantum number n+1.

in units of 10^{-15} cm^2 with E in ev

$$Q_{2,3}\ (E+E_{ex}) = 9.3 \times \sqrt{E}$$

$$Q_{3,4}\ (E+E_{ex}) = 73 \times \sqrt{E}$$

$$Q_{4,5}\ (E+E_{ex}) = 380 \times \sqrt{E}$$

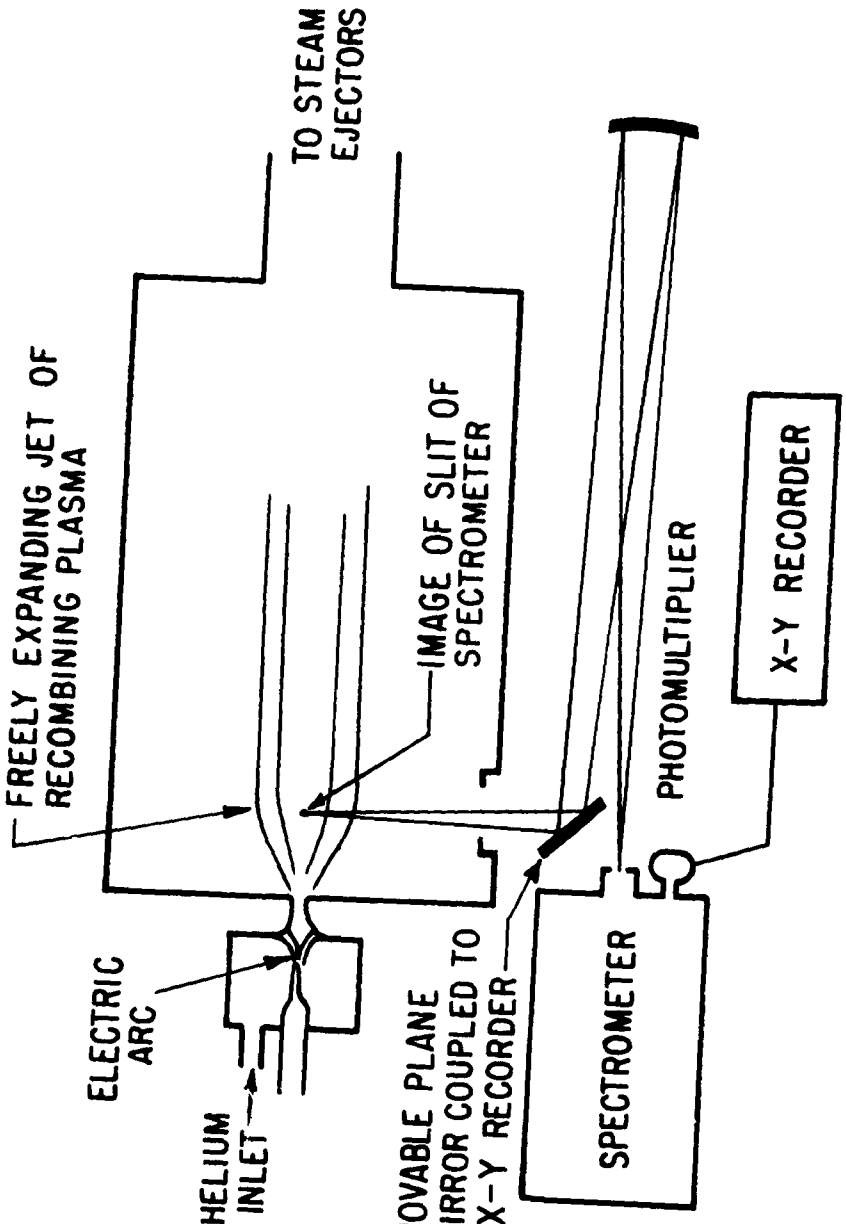

FIG. 1. SCHEMATIC OUTLINE OF PLASMA JET WIND TUNNEL AND SPECTROMETER OPTICS

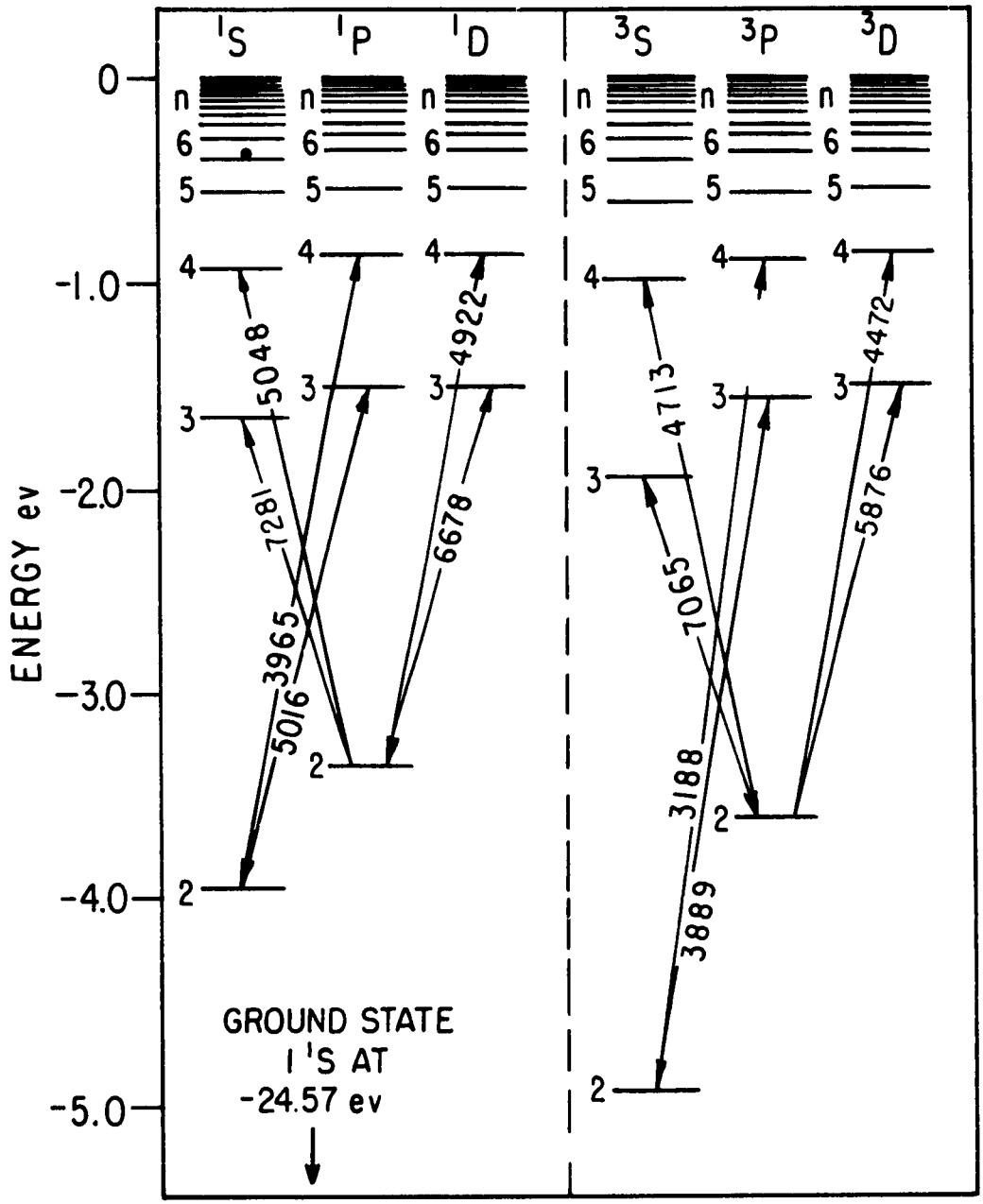

FIG. 2. ENERGY LEVEL DIAGRAM FOR HELIUM

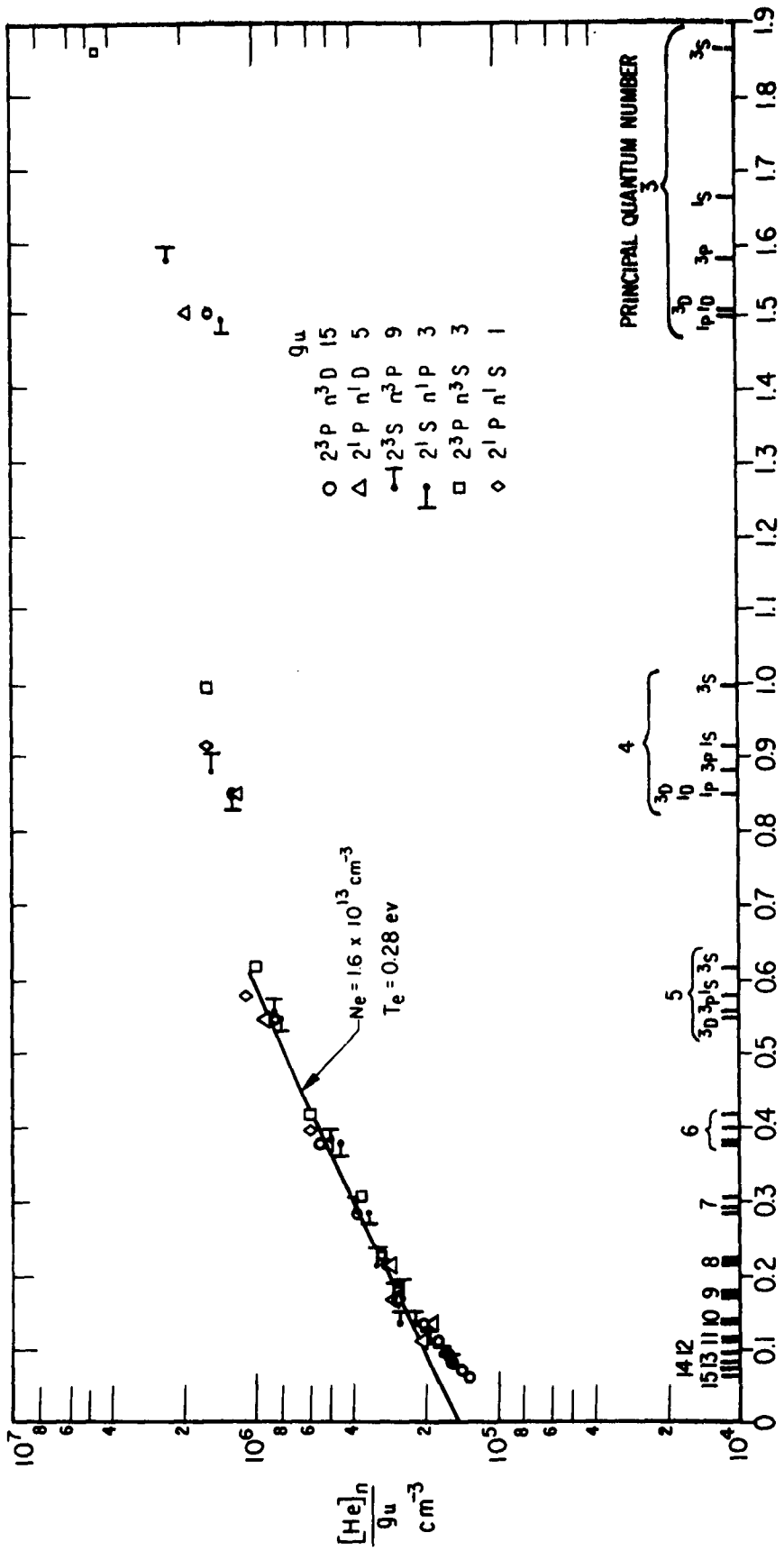

FIG. 3. DENSITY OF EXCITED STATES OF HELIUM

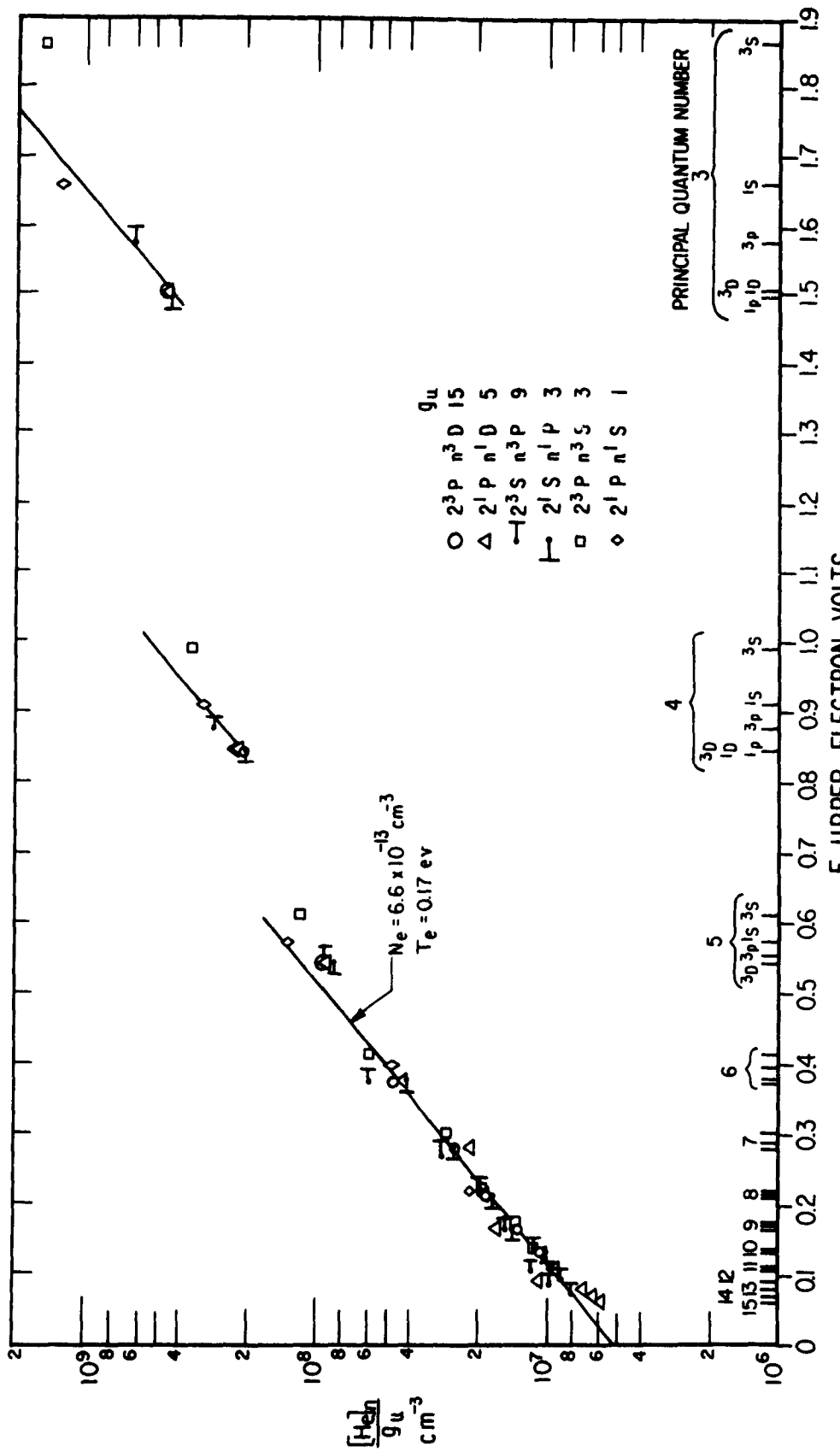

FIG. 4. DENSITY OF EXCITED STATES OF HELIUM

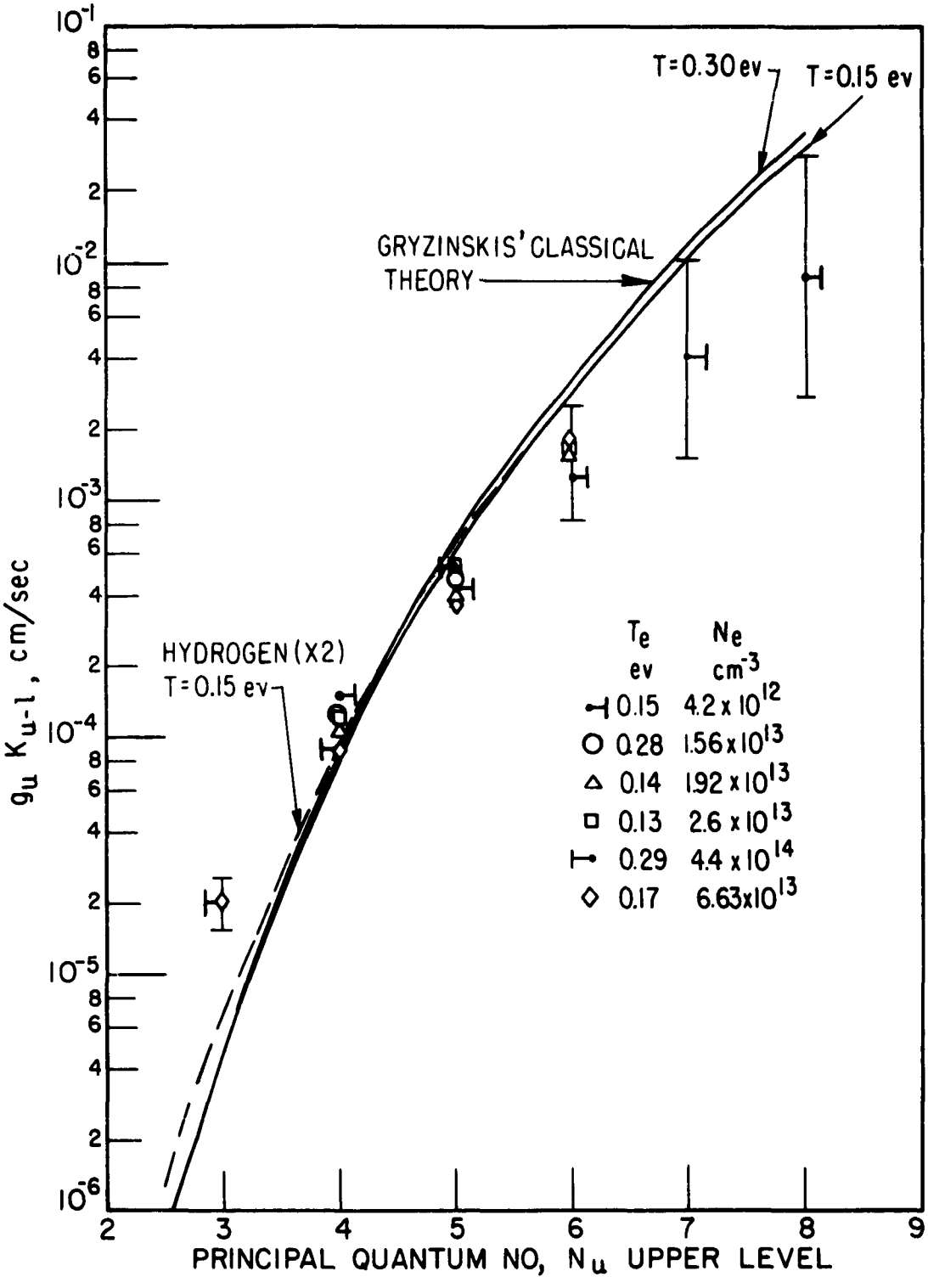

FIG. 5. COLLISIONAL DE-EXCITATION RATE CONSTANTS FOR HELIUM

APPENDIX A

THE NUMERICAL SOLUTION OF THE ABEL INTEGRAL EQUATION

As shown in Fig. A1, the spectrograph observes all the radiation along line L emitted in a solid angle Ω. This radiation will be given by

$$J(x) = \int_{-y_o}^{+y_o} I(x,y)\, dy \qquad (A1)$$

where $I(x,y)$ is the intensity per unit solid angle of emission at a point x,y in the plasma, the limits extending to the edge of the plasma. If $I(x,y)$ is in watts/cm^3 steradian, then $J(x)$ will be in watts/cm^2 steradian. If the plasma is assumed to by cylindrically symmetric about $x = y = 0$, then I is a function only of $r = (x^2 + y^2)^{1/2}$. Upon changing the variable of integration in Eq. (A1) to r, there results

$$J(x) = 2 \int_{x}^{R} \frac{I(r)\, r\, dr}{(r^2 - x^2)^{1/2}} \qquad (A2)$$

where R gives the radius of the plasma at the edge. This is called a Volterra integral equation of the first kind.[21] Since the kernel has a singularity at one of the end points, the standard techniques of solving such equations cannot be used until a transformation is applied to Eq. (A2) which removes this singularity.[22] When this is done, and the inversion transformed back to the original functions, there results

$$I(r) = -\frac{1}{\pi} \int_{r}^{R} \frac{\frac{dJ(x)}{dx}\, dx}{(x^2 - r^2)^{1/2}} \qquad (A3)$$

Unless $J(x)$ is an appropriate analytic function, it is necessary to use numerical techniques to solve this equation.

When $J(x)$ is given as a table, J_n, of experimentally determined points, the most obvious technique is to break Eq. (A3) into a sum of integrals, with each integral covering the region between two entries in the table of J_n. Some analytic interpolating function is then used to represent $J(x)$ in the region between the points, the integral in Eq. (A3) is performed, and the result can be represented as

$$I_m = \frac{1}{h} \sum_{n=0}^{N} J_n Z_{nm} \quad , \tag{A4}$$

where the radius of the plasma has been divided into N intervals of size h, such that $x = nh$ and $r = mh$.

Choosing the interpolating function as a polynomial of third order, we let

$$J(x) = A_n x^3 + B_n x^2 + C_n x + D_n \tag{A5}$$

represent the value of $J(x)$ between $x = nh$ and $x = (n+1)h$. The constants are evaluated from J_{n-1}, J_n, J_{n+1}, J_{n+2}, except that for $n = 0$ the condition $\frac{dJ(x)}{dx} = 0$ at $x = 0$ is substituted for J_{n-1}. Substituting Eq. (A5) in Eq. (A3) there results

$$I(mh) = -\frac{1}{\pi} \sum_{n=0}^{N} \int_{nh}^{(n+1)h} \frac{[3A_n x^2 + 2B_n x + C_n]dx}{(x^2 - mh)^{1/2}} \tag{A6}$$

When the integrals in Eq. (A6) are carried out, and the values of A_n, B_n, and C_n in terms of J_n are substituted, it is found that all terms in J_o, J_1, etc., can be collected. Eq. (A6) can then be put in the form

$$I(mh) = \frac{1}{h} \sum_{n=0}^{N} J_n Z_{nm} \quad . \tag{A6}$$

The values of $Z_{n,m}$ were calculated on an IBM 1620, and the values up to $n = 20$ for $m = 0$ are given in Table AI. These values are the same as those given by Bockasten,[9] except that he chose a different manner of fitting the interpolating function at the edge of the plasma, giving somewhat different values for the last two entries of $Z_{n,m}$. The resulting difference in the calculated value of $I(r)$ near the centerline is negligible.

If a linear interpolating function is used in place of Eq. (A5), then somewhat different values of $Z_{n,m}$ are found. Values for $m = 0$, taken from Nestor and Olsen,[8] are given in Table AI. If the values of J_n are accurate enough, use of the coefficients $Z_{n,m}$ derived from a linear rather than a cubic interpolating function will always give less accurate values of I_m. However, as can be seen from Table AI, A_{nm} linear introduces less cancelation near the center of the values of J_n than Z_{nm} cubic, so that if the values of J_n are not too accurate, and a large number of points are used, more accurate results may be obtained by use of Z_{linear}. In this case, though, either graphical or analytic smoothing of the points will increase the accuracy. A least squares technique, applied to the whole profile $J(x)$ as discussed by Freeman and Katz,[10] or to several groups of points as discussed by Bockasten,[9] can be used to give analytic smoothing. If the values of J_n are sufficiently accurate, however, use of a smoothing technique may reduce the accuracy of I_m.

A smoothing technique based on the use of an incomplete Fourier cosine series representation of $J(x)$[11] was tried and compared in accuracy to the use of Z_{nm} cubic. This method is equivalent to least squares smoothing applied to the whole profile $J(x)$.

Equation (A5) is replaced by

$$J(x) = \sum_{a=0}^{k} f_a \cos \frac{a\pi x}{R} , \quad 0 \leq |x| \leq R \tag{A7}$$

where f_a are given by the normal Fourier inversion,

$$f_a = \frac{2}{R} \int_0^R J(x) \cos \frac{a\pi x}{R} \, dx , \quad (a \neq 0) . \tag{A8}$$

Upon inserting Eq. (A7) in Eq. (A3), there results,

$$I(r) = \frac{1}{R} \sum_{a=0}^{k} a \, f_a \, B_a \, (r/R) , \tag{A9}$$

with

$$B_a(\rho) = \int_\rho^1 \frac{\sin a\pi u}{(u^2 - \rho^2)^{1/2}} \, du .$$

Equation (A8) is then evaluated using the trapezoidal rule with the given values of $J(x) = J_n$,

$$f_a = \frac{2}{N} \left[J_o/2 + \sum_{n=1}^{N} J_n \cos (a\pi n/N) \right].$$

This is substituted in Eq. (A9) and the order of summation reversed, resulting in

$$I_m = \frac{1}{h} \sum_{n=0}^{N} J_n Z_{n,m} \qquad \text{(A10)}$$

with

$$Z_{n,m} = 2 \sum_{a=1}^{k} a B_a (m/N) \cos (a\pi n/N) \quad , \quad n \neq 0$$

and

$$Z_{o,m} = \sum_{a=1}^{k} a B_a (m/N) \quad .$$

Values of $Z_{n,o}$ given by Shumaker[11] for $k = 6$ and $N = 20$ are presented in Table AI. It is seen that the values of I_m calculated with these coefficients are less sensitive to errors in J_n.

The accuracy of the values of I_m calculated with these different tables of Z_{nm} was studied by trying them on a function which approximated the experimentally measured $J(x)$, and whose inversion could be obtained analytically. The function chosen was

$$J(x) = 8 (1 - x^2)^{3/2}$$

whose inversion is

$$I(r) = 6 (1 - r^2)$$

$J(x)$ was divided into 5, 10, and 20 points, and the accuracy was varied by rounding off to 4, 3, and 2 significant figures. For two significant figures of accuraty, which was estimated to be the error in reading the traces in these experiments, calculation of I_m using 20 points and Z_{nm} Fourier was comparable in accuracy to using five points and Z_{nm} cubic. The error was about 2% near the centerline in this case. If 20

points and Z_{nm} cubic were used, the error was much larger, about 20%. However, when $J_n(x)$ was given to four significant figures, the error in I_m using 20 points and Z_{nm} Fourier was still about 2%, while the error using Z_{nm} cubic with 20 points was less than 0.1%. In all cases use of Z_{nm} linear resulted in less accuracy than use of Z_{nm} cubic.

Some of the experimental results were evaluated with Z_{nm} Fourier as well as Z_{nm} cubic, and no significant increase in accuracy was noted. Probably the smoothing introduced by eye when reading the values of J_n from the charts, coupled with division of $J(x)$ into about seven points, is sufficient to give about maximum attainable accuracy.

TABLE AI

COEFFICIENTS FOR THE ABEL INTEGRAL INVERSION

in units of 10^{-2}

n	Z_{no}, cubic interpolation	Z_{no}, linear interpolation	Z_{no}, Fourier interpolation
0	76.258	63.661	8.240
1	-58.007	-42.443	12.481
2	- 5.847	- 8.488	3.020
3	- 3.395	- 3.635	- 6.090
4	- 1.970	- 2.018	- 9.772
5	- 1.269	- 1.286	- 6.994
6	- 0.883	- 0.891	- 1.013
7	- 0.649	- 0.656	3.403
8	- 0.497	- 0.499	3.521
9	- 0.393	- 0.395	0.281
10	- 0.318	- 0.318	- 2.988
11	- 0.263	- 0.263	- 3.504
12	- 0.222	- 0.222	- 1.156
13	- 0.188	- 0.188	1.748
14	- 0.162	- 0.162	2.677
15	- 0.141	- 0.141	1.026
16	- 0.125	- 0.125	- 1.548
17	- 0.110	- 0.110	- 2.749
18	- 0.098	- 0.098	- 1.695
19	- 0.088	- 0.088	0.398
20	- 0.081	- 0.081	--

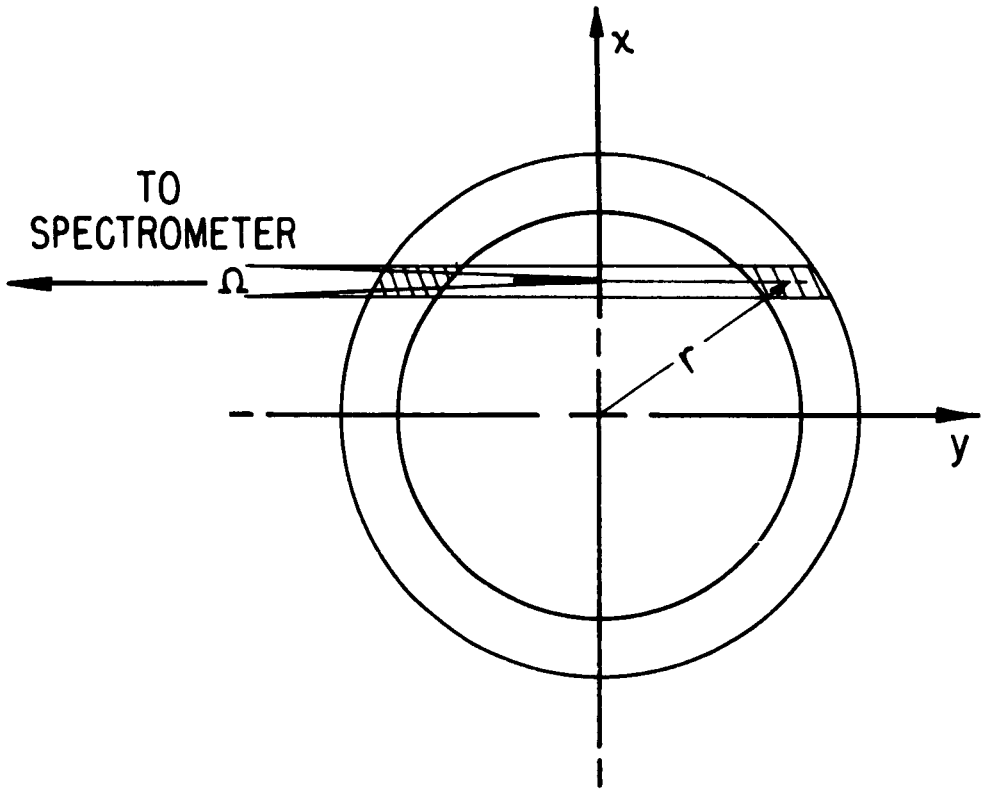

FIG. A1. DIAGRAM OF PORTION OF CYLINDRICALLY SYMMETRIC PLASMA VIEWED BY SPECTROMETER

APPENDIX B

THE MEASUREMENT OF THE INTENSITY OF AN ATOMIC LINE

Einstein assumed that an atom in an excited state u has a certain probability per unit time, $A_{u\ell}$, of making a spontaneous transition with emission of radiation to state ℓ of lower energy.[23] With the development of quantum theory it became possible to compute from first principles the value of $A_{u\ell}$ for simple systems. The intensity of an atomic line is given by

$$I_{u\ell} = N_u \frac{A_{u\ell}}{4\pi} (E_u - E_\ell) \qquad \text{(B1)}$$

in ergs/(cm^3-sec-steradian), with N_u the number/cm^3 of atoms in the upper state and $E_u - E_\ell$ the energy of the quantum of radiation. Absorption and induced emission are neglected in this formula. Thus, if $A_{u\ell}$ is known, measurement of $I_{u\ell}$ will lead to a value of N_u.

First it is noted that the wavelength of the transition from state u to state ℓ is not perfectly monochromatic, but is spread over a wavelength range $\Delta\lambda$ by various line broadening phenomena. In these experiments Doppler broadening is the most important for the low lying levels of helium, while the electric microfields due to nearby electrons and ions cause a large broadening of the levels of helium near the ionization limit. These line broadening phenomena do not change the mean radiative lifetime of the upper state appreciably, so that Eq. (B1) still holds, with $I_{u\ell}$ considered to be all the radiation associated with the line. The spectrometer responds to the radiation falling on the entrance slit, $J(\lambda)$ in ergs/(cm^2-sec-Angstrom-steradian), which

must be first integrated over the line width $\Delta\lambda$ corresponding to the transition $u \rightarrow \ell$,

$$J'_{u\ell} = \int_{\Delta\lambda} J_{u\ell}(\lambda)\, d\lambda \qquad (B2)$$

and then the Abel integral inversion, Eq. (2), must be performed on $J'_{u\ell}$ to find $I_{u\ell}$ of Eq. (B1). The Abel integral inversion in effect finds the mean depth D of the emitting plasma, which gives $I_{u\ell}$ as

$$I_{u\ell} = J'_{u\ell}/D \quad . \qquad (B3)$$

The magnitude of the photomultiplier current when the spectrometer is set at wavelength λ can be given by

$$R(\lambda) = \int_{\Delta\lambda} g(\lambda-\lambda')\, J_{u\ell}(\lambda')\, d\lambda' \quad , \qquad (B4)$$

where $g(\lambda-\lambda')$ is the response function of the spectrometer and is different from zero for only a small range of wavelength around λ. Its shape is determined by the entrance and exit slit widths and the aberrations of the spectrometer, and its magnitude principally by the sensitivity of the photomultiplier and transmissivity of the spectrometer. When the spectrometer is focused on the standard tungsten filament lamp, its signal will be

$$R^\circ(\lambda) = \int g(\lambda-\lambda')\, J^\circ(\lambda')\, d\lambda' = J^\circ(\lambda) \int g(\lambda-\lambda')\, d\lambda' \quad ,$$

where $J^\circ(\lambda')$ is the known spectral steradiancy of the standard lamp,

and can be taken out of the integral since it will be constant over the wavelength range where $g(\lambda-\lambda')$ differs from zero. Thus the sensitivity of the spectrometer,

$$S(\lambda) = R^{\circ}(\lambda)/J^{\circ}(\lambda) \quad , \tag{B6}$$

is determined, and a typical graph of this versus wavelength is shown in Fig. B1. When the spectrometer is focused on the plasma, and the wavelength is set to receive radiation from transition $u\ell$, the signal is

$$R_{u\ell}(\lambda_o) = \int_{\Delta\lambda} g(\lambda_o-\lambda')\, J_{u\ell}(\lambda')\, d\lambda' = g(\lambda_o-\lambda') \int_{\Delta\lambda} J_{u\ell}(\lambda')\, d\lambda' \quad , \tag{B7}$$

where the response function $g(\lambda_o-\lambda')$ has been assumed to have a constant value over the width $\Delta\lambda'$ of the line. This was achieved in the present experiment by having an entrance slit width of 0.71 mm, resulting in a reasonably uniform response function over a wavelength range of 3 A. If in Eq. (B7) the line width is small compared to changes in $g(\lambda-\lambda')$, the line acts as a delta function in picking out a value of λ', and $R_{u\ell}(\lambda)$ will be a faithful representation of $g(\lambda-\lambda')$. Upon producing a curve of $R_{u\ell}(\lambda)$ by scanning the spectrometer slowly over a narrow line, and integrating the resulting trace with a planimeter, there results

$$\frac{\int R_{u\ell}(\lambda)\, d\lambda}{R_{u\ell}(\lambda_o)} = \frac{\int g(\lambda-\lambda')\, d\lambda'}{g(\lambda_o-\lambda')} = W \quad , \tag{B8}$$

where $R_{u\ell}(\lambda_o)$ is the value of the curve at its flat top. W is called the spectral slit width, in Angstroms, and is independent of λ within

the experimental error. It can now be seen that

$$J'_{u\ell} = \int_{\Delta\lambda} J_{u\ell}(\lambda)\, d\lambda = \frac{R_{u\ell}(\lambda_o) \times W}{S(\lambda_o)} \quad , \tag{B9}$$

which is identical with Eq. (5).

W was determined using the singlet lines of helium from a discharge tube in several regions of the spectrum, and did not vary by more than 5%. The width of these lines is about 0.07 A, while $g(\lambda-\lambda')$ has a flat top about 3 A wide, so that the approximations leading to Eq. (B8) are well satisfied. Equation (B9) will correctly describe the intensity of a line emitted from the plasma as long as the width of the line is somewhat less than 3 A.

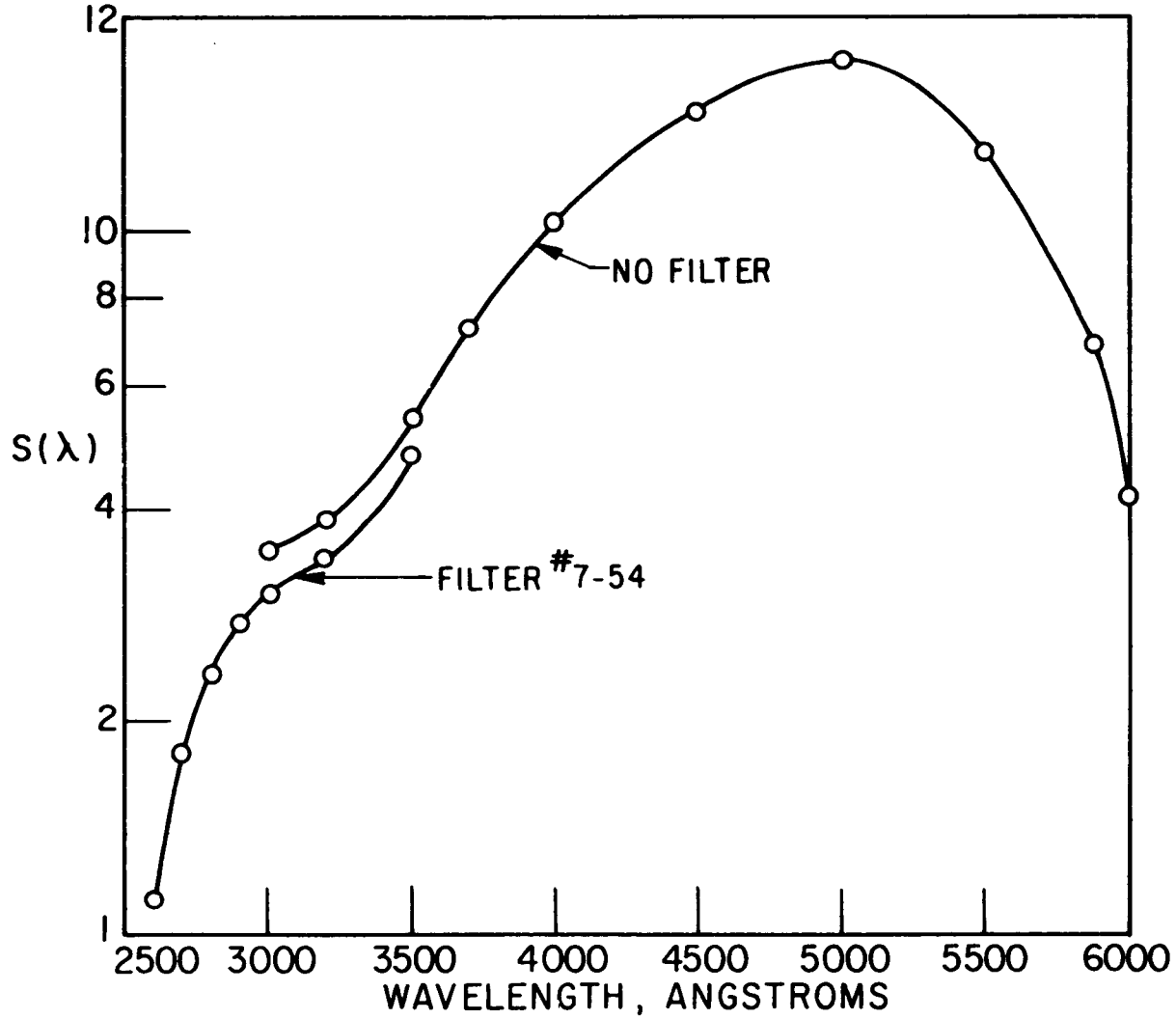

FIG. B1. SPECTRAL SENSITIVITY OF SPECTROMETER, S(λ), IN UNITS 10^{-8} amps/[μ watt/(ster-millimicron-mm^2)]

AIR FORCE

ASTIA (10)
ATTN: TIPCR
Arlington Hall Station
Arlington 12, Virginia

AFOSR
ATTN: SRHM (2)
ATTN: SRGL (2)
Washington 25, D. C.

EOOAR (2)
Shell Building
47 Rue Cantersteen
Brussels, Belgium

AEDC
ATTN: AEOIM
Arnold Air Force Station
Tennessee

AFFTC
ATTN: FTOTL
Edwards AF Base
California

ARMDC
ATTN: HDOI
Holloman AF Base
New Mexico

AFMTC
ATTN: AFMTC Tech Library-MU-135
Patrick AF Base
Florida

AFOSR (SRLTL)
Holloman AF Base
New Mexico

Aeronautical Systems Division
ATTN: WWAD (2)
ATTN: WWRMCM (1)
ATTN: ASRNGC (1)
Wright-Patterson AF Base, Ohio

ARL (OAR) (2)
Wright-Patterson AF Base
Ohio

Institute of Technology Library (AU)
MCLI-LIB, Bldg. 125, Area B
Wright-Patterson AF Base, Ohio

APGC (PGAPI)
Eglin AF Base
Florida

AFCRL
ATTN: CRRELA (2)
Bedford, Massachusetts

AFSWC (SWOI)
Kirtland AF Base
New Mexico

ARMY

Director BRL
ATTN: Library
Aberdeen Proving Ground, Maryland

Office of Ordnance Research
Box CM
Duke Station
Durham, North Carolina

Army Rocket and Guided Missile Agency
ATTN: Technical Library
Redstone Arsenal, Alabama

Signal Corps Engineering Laboratory
ATTN: SIGFMIEL - RPO
Fort Monmouth, New Jersey

Office of the Chief of R&D
ATTN: Scientific Information
Department of the Army
Washington, 25, D.C.

NAVY

Office of Naval Research (2)
ATTN: Mechanics Branch (1)
Airbranch (1)

Naval Research Laboratory
ATTN: Documents Library
Washington 25, D. C.

Naval Ordnance Laboratory
ATTN: Library
White Oak, Maryland

David Taylor Model Basin
Aerodynamics Laboratory
ATTN: Library
Washington 7, D.C.

Chief, Bureau of Ordnance
Department of the Navy
ATTN: Special Proj.Off, SP-2722
Washington 25, D.C.

OTHER GOVERNMENT

NASA
ATTN: Document Library
1502 H Street, N.W.
Washington 25, D. C.

Ames Research Center (NASA)
ATTN: Technical Library
Moffett Field, California

AFOSR (2)
ATTN: SRHM
ATTN: SRGL
Washington 25, D.C.

High Speed Flight Station (NASA)
ATTN: Technical Library
Langley AFB, Virginia

Lewis Research Center (NASA)
ATTN: Technical Library
21000 Brookpark Road
Cleveland 35, Ohio

National Bureau of Standards
U.S. Department of Commerce
ATTN: Technical Reports Section
Washington 25, D. C.

Office of Technical Services
U.S. Department of Commerce
ATTN; Tech. Reports Section
Washington 25, D.C.

National Science Foundation
ATTN; Eng. Sciences Division
1951 Constitution Ave., NW
Washington 25, D.C.

U.S. Atomic Energy Commission
Tech. Information Extension
P.O. Box 62
Oak Ridge, Tennessee

U.S. Atomic Energy Commission
Technical Information Service
1901 Constitution Ave., NW
Washington 25, D. C.

Lewis Research Center (NASA)
ATTN; Technical Library
21000 Brookpark Road
Cleveland 35, Ohio

JOURNALS

Southwest Research Institute (2)
ATTN: Applied Mechanics Review
San Antonio 6, Texas

Aeronautical Engineering Review
2 East 64th Street
New York 21, New York

Institute of Aeronautical Sciences
ATTN: Library
2 East 64th Street
New York 21, New York

FOREIGN ORGANIZATIONS

Chairman
Canadian Joint Staff (DRB/DSIS)
2451 Massachusetts Avenue, NW
Washington 25, D. C.

Director
National Aeronautical Establishment
Ottawa, Ontario
Canada

University of Toronto
Institute of Aerophysics
ATTN: Library
Toronto 5, Canada

Training Center for Experimental
Aerodynamics
ATTN: Library
Rhode-Saint-Genese (Belgique)
72, Chaussee de Waterloo,
Brussels, Belgium

Library (Route to Dr.W.P.Jones)
Aeronautical Research Council
National Physical Laboratory
Teddington, England

EDUCATIONAL INSTITUTES

Aeronautical Research Associates
of Princeton
50 Washington Road
Princeton, New Jersey

Auburn University
Dept. of Mechanical Engineering
Auburn, Alabama

Brown University
Gifts and Exchanges Library
Providence 12, Rhode Island

University of California
Institute of Engineering Research
Low Pressures Research Project
Berkeley 4, California

University of California
Engineering Department
ATTN: Library
Los Angeles 24, California

California Institute of Technology
ATTN: JPL Library
2800 Oak Grove Drive
Pasadena 4, California

California Institute of Technology
Guggenheim Aeronautical Laboratory
ATTN: Aeronautical Library
(Route to Prof.Liepmann)
Pasadena 4, California

Colorado State University
Department of Civil Engineering
ATTN; Prof. J. E. Cermak, ASCE
FORT Collins, Colorado

Columbia University
Department of Civil Engineering
& Engineering Mechanics
ATTN: Library (Route to
Prof. G. Herrmann)
New York 27, New York

Cornell University
Graduate School of
Aeronautical Engineering
ATTN: Library (Route to
Prof. W.R.Sears)
Ithaca, New York

Harvard University
Dept. of Engineering Sciences
ATTN: Library
Cambridge 38, Massachusetts

John Crerar Library
86 E. Randolph Street
Chicago 1, Illinois

The Johns Hopkins University
Applied Physics Lab Library
8621 Georgia Avenue
Silver Spring, Maryland

The Johns Hopkins University
Department of Mechanics
ATTN: Library (Route to
Profs. Clauser & Corrsin)
Baltimore 18, Maryland

University of Maryland
Institute for Fluid Dynamics
and Applied Mechanics
College Park, Maryland

Massachusetts Institute of
Technology
Naval Supersonic Laboratory
Cambridge 39, Massachusetts

Massachusetts Institute of
Technology
ATTN: Aeronautics Library
Cambridge 39, Massachusetts

Midwest Research Institute
ATTN: Library
425 Volker Boulevard
Kansas City 10, Missouri

Rosemount Aeronautical Labs.
University of Minnesota
ATTN: Library
Minneapolis, Minnesota

North Carolina State College
Div. of Engineering Research
ATTN: Technical Library
Raleigh, North Carolina

Ohio State University
Dept. of Aeronautical Engineering
ATTN: Library
Columbus, Ohio

Polytechnic Institute of Brooklyn
ATTN: Library
333 Jay Street
Brooklyn 1, New York

Aerodynamics Laboratory
Polytechnic Institute of Brooklyn
527 Atlantic Avenue
Freeport Long Island, New York

The James Forrestal Research Center
Princeton University
ATTN: Library (Route to
Prof.S.Bogdonoff)
Princeton, New Jersey

Princeton University
Dept. of Aeronautical Engineering
ATTN: Library
Princeton, New Jersey

Rensselaer Polytechnic Institute
Dept. of Aeronautical Engineering
ATTN; Library
Troy, New York

University of Southern California
Engineering Center (Library)
3518 University Avenue
Los Angeles 7, California

Stanford Research Institute
Documents Center
ATTN: Acquisitions)
Menlo Park, California

Stanford University
Dept. of Aeronautical Engineering
ATTN: Library
Stanford, California

Defense Research Laboratory
University of Texas
P.O.Box 8029
Austin 12, Texas

University of Virginia
Ordnance Research Laboratory
Charlottesville, Virginia

University of Washington
Department of Aeronautical
Engineering
ATTN: Library
Seattle, Washington

New York University
Institute of Mathematical Sciences
ATTN; Library
New York 3, New York

Yale University
Department of Mechanical
Engineering
ATTN: Library (Route to
Dr. P. Wegener)
New Haven 10, Connecticut

INDUSTRIAL ORGANIZATIONS

AVCO-Everett Research Laboratory
ATTN; Research Library (Route
to F.R.Riddell)
201 Lowel Street
Wilmington, Massachusetts

AVCO-Everett Research Lab.
ATTN; Technical Library
(Route to Petschek)
2385 Revere Beach Parkway
Everett 49, Massachusetts

Boeing Scientific Research Labs.
ATTN: Research Library
P.O. Box 3981
Seattle 24, Washington

Chance-Vought Aircraft, Inc.
ATTN: Library
Dallas, Texas

Convair
Forth Worth Division
ATTN: Library
Fort Worth 1, Texas

Convair - San Diego
ATTN: Engineering Library
San Diego 12, California

Convair Scientific Research Lab.
ATTN: Library (Route to Chief,
Applied Research)
P.O. Box 950
San Diego 12, California

Cornell Aeronautical Labs, Inc.
ATTN: Library
4455 Genessee Street
Buffalo 21, New York

Douglas Aircraft Company, Inc.
ATTN: Library
827 Lapham Street
El Segundo, California

Douglas Aircraft Company, Inc.
ATTN: Library
3000 Ocean Park Boulevard
Santa Monica, California

Flight Sciences Laboratory
ATTN: Library (Route to
Dr. J.Isenberg)
1965 Sheridan Avenue
Buffalo 23, New York

General Atomic
ATTN: Library
P.O. Box 608
San Diego 12, California

General Applied Science
Laboratories, Inc.
ATTN: Library (Route to
Drs. Merrick, Stewart
& Arnold)
Westbury, New York

General Electric Company
Gas Turbine Division
ATTN: Library (Route to
Dr. Ghai)
Cincinnati 15, Ohio

General Electric Company
Research Laboratory
P.O. Box 1088
Schenectady 5, New York

Grumman Aircraft Engineering
Corporation
ATTN: Library
Bethpage Long Island, New York

Hughes Aircraft Company
Research & Development Labs.
ATTN: Library
Culver City, California

Dr. J. Lukasiewicz, Chief
von Karman Gas Dynamics Facility
ARO, Inc.
Arnold Air Force Station, Tenn.

The Martin Company
ATTN; Library
Denver, Colorado

The Martin Company
ATTN: Library
Baltimore 3, Maryland

Lockheed Aircraft Corporation
ATTN: Library
P.O. Box 551
Burbank, California

McDonnell Aircraft Corp.
ATTN: Library
P.O. Box 516
St. Louis 66, Missouri

North American Aviation, Inc.
Missile Division
ATTN: Library
12214 Lakewood Boulevard
Downey, California

Northrop Aircraft, Inc.
ATTN: Library
Hawthorne, California

Rand Corporation
1700 Main Street
Santa Monica, California

Republic Aviation Corporation
ATTN: Library
Farmingdale Long Island, New York

United Aircraft Corporation
Research Department (Library)
400 Main Street
East Hartford 8, Connecticut

Unified Science Associates, Inc.
ATTN: S.Naiditch, President
926 S. Arroyo Parkway
Pasadena, California

Vitro Laboratories
ATTN: Library (Route
to Dr. Sheer)
200 Pleasant Valley Way
West Orange, New Jersey

Westinghouse Electric Corp.
ATTN: Library
306 4th Avenue
Pittsburgh, Pennsylvania

MSVD Library
General Electric Company
Valley Forge Space Technology Center
King of Prussia, Pennsylvania
ATTN: L. Chasen, Manager - Library
M/F Dr. F.W.Wendt

Dynatech Corporation
17 Tudor Street
Cambridge, Massachusetts
ATTN: Mr. Robert E. Goode